Energetic-ion Confinement Studies by Using Comprehensive Neutron Diagnostics in the Large Helical Device

K. Ogawa[1,2], M. Isobe[1,2], T. Nishitani[1], S. Murakami[3], R. Seki[1,2], H. Nuga[1], S. Kamio[1], Y. Fujiwara[1], H. Yamaguchi[1], Y. Saito[3], S. Maeta[3], M. Osakabe[1,2], and LHD Experiment Group[1]

[1]National Institute for Fusion Science, National Institutes of Natural Sciences, Toki, Japan.

[2]SOKENDAI (The Graduate University for Advanced Studies), Toki, Japan.

[3]Kyoto University, Kyoto, Japan.

kogawa@nifs.ac.jp

Abstract

Understanding of energetic particle (EP) confinement is one of the critical issues in realizing fusion reactor. In stellarator/helical devices, the research on EP confinement is one of the key topics to obtain better confinement by utilizing the flexibility of three-dimensional magnetic field. Study of EP transport in the Large Helical Device (LHD) has been performed by means of escaping EP diagnostics in hydrogen plasma operation. By starting deuterium operation of the LHD, confinement study of EPs has progressed remarkably by using newly developed comprehensive neutron diagnostics providing the information of EPs confined in the core region. The total neutron emission rate (S_n) increases due to the relatively low deviation of beam ion orbit from the flux surface with the inward shift of the magnetic axis. S_n has the peak around the electron density of 2×10^{19}m^{-3} to 3×10^{19}m^{-3}, as predicted. It is found that the fraction of beam-beam components in S_n is evaluated to be approximately 20% by the Fokker-Planck models TASK/FP in the plasma with both co- and counter-neutral beam injections. The equivalent fusion gain in DT plasma achieved 0.11 in a negative-ion-based neutral beam heated

plasma. Time evolution of S_n following the short pulse neutral beam injection into the electron-cyclotron-heated low-beta plasma is reproduced by drift kinetic simulation, indicating that transport of beam ion injected by short pulse neutral beam can be described with neoclassical models in magnetohydrodynamic quiescent low-beta plasmas. The vertical neutron camera works successfully, demonstrating that in the co-neutral beam injected plasma, neutron emission profile shifts according to magnetic axis position. The shift of the neutron emission profile is reproduced by orbit-following models. The triton burnup study is performed for the first time in stellarator/heliotron so as to understand the alpha particle confinement. It is found that the triton burnup ratio, which largely increases at inward shifted configurations due to the better triton orbit and better plasma performance in inward shifted configuration is similar to that measured in tokamak having a similar minor radius with the LHD. We study the confinement capability of EPs toward a helical reactor in magnetohydrodynamic -quiescent region and expansion of the energetic-ion physics study in toroidal fusion plasmas.

1. Introduction

One of the issues for realizing a fusion reactor is how to sustain the high performance plasma by self-heating using fusion born alpha particles [1]. In order to understand the alpha particle confinement in a fusion reactor, much attention has been given to studying the energetic ion physics in existing fusion plasma devices using energetic particles produced by neutral beam injections and/or ion cyclotron resonance frequency heating, especially in middle and large tokamaks [2]. Although the plasma performance of the stellarator and the helical systems do not exceed the performance achieved in tokamaks, stellarators and helical systems have the advantage of steady-state operation because of the absence of disruption. Recently, the performance of stellarators and helical devices increased dramatically. For example, the

achievement of 10 keV ion temperature in LHD [3] and the stored plasma energy exceeds 6×10^{26} Celsius m^{-3} s in Wendelstein 7-X [4]. In stellarators and helical systems, the energetic particle confinement study has been led by the Large Helical Device (LHD) using intensive neutral beam (NB) injection [5-7]. In hydrogen experiments, the study of energetic ion confinement is mainly performed by the measurement of energetic particle that escaped from the plasma confinement region using a neutral particle analyzer and fast ion loss detector [8-10]. Study of beam ion transport/loss due to toroidal Alfvén eigenmode, energetic particle mode and pressure-driven magnetohydrodynamic modes were reported [11-16].

In order to achieve higher performance plasma, deuterium plasma campaign in LHD was planned in the initial phase of LHD project [17]. In this plan, not only obtaining higher performance plasma, but also expansion of energetic particle study were expected. Prediction of the total neutron emission rate (S_n) was conducted using the Fokker-Planck numerical simulation. The simulation results showed that S_n from the LHD plasma is order of 10^{16} n/s and most of the neutrons are created by reactions between beam ions and bulk plasma the so-called called beam-thermal components [18-20]. Therefore, information of energetic particles such as global confinement of energetic particles, the radial profile of energetic particles and the energy spectra of energetic particles can be obtained using neutron diagnostics. The total neutron emission rate from the LHD is the same order as the total neutron emission rate in deuterium discharge conducted in large tokamaks. Therefore, the advanced study of energetic particles performed in the large tokamaks is expected in the stellarators and the helical systems using the LHD. To conduct the energetic particle study, developments and prior evaluations of the neutron flux monitor [21-24], the neutron camera based on scintillation detector [25-28] and based on the nuclear emulsion [29-32], neutron energy spectrometer [33-34] have been performed. Furthermore, the simulation of 3.5 MeV alpha particle confinement using 1 MeV tritons created by DD reactions is possible for the first time in the stellarator/heliotron devices.

To obtain shot-integrated DD and secondary created DT neutron fluence and evaluate shot-integrated triton burnup ratio, neutron activation system was planned to be installed [8]. To measure the time evolution of secondary created DT neutron, scintillating fiber detectors has been developed [35-37]. Also, a predictive study of 1 MeV triton confinement study based on numerical simulations has been performed in advance of the deuterium operation of the LHD [38]. It was shown that the higher triton burnup ratio is expected in inward shifted configurations compared with outward shifted configurations. Recently, comprehensive neutron diagnostics have been installed for the deuterium operation of the LHD initiated in March 2017. The initial results of LHD deuterium operation using neutron diagnostics were reported [39]. The neutron diagnostics work well, as planned in the first deuterium plasma campaign of the LHD. The deuterium operation of the LHD provides us the opportunity to extend the study of the energetic particle physics based on confined energetic-particle measurement. This paper reports the energetic ion confinement study using the comprehensive neutron diagnostics performed in the first campaign of deuterium plasma operation in the LHD.

2. Neutron Diagnostics in the Large Helical Device

For the deuterium operation of LHD plasma, comprehensive neutron diagnostics were prepared and the commissioning of those diagnostics was performed [40, 41]. The comprehensive neutron diagnostics in the first LHD deuterium campaign are shown in Fig. 1. The neutron flux monitor, the neutron activation system, the vertical neutron camera, and scintillating-fiber detectors are used for obtaining S_n, total DD and secondary DT neutron emission amount, neutron emission profiles, and time evolution of the DT neutron emission rate, respectively. The time evolution of S_n is obtained by the absolutely-calibrated neutron flux monitor consisting of fission chambers and ^{3}He/^{10}B proportional counters [21]. The digital signal

processing unit is developed for the fission chamber equipped with the field programmable logic circuit realizing the wide dynamic range up to 5×10^9 cps and finer temporal resolution of 2 ms. Study of global confinement of beam ions will be enhanced by means of the neutron flux monitor. The vertical neutron camera consists of the multichannel collimator, fast-neutron scintillation detectors, and the fast analog to digital converter equipped with field programmable logic controller gives the radial neutron emission profile [28]. The multichannel collimator is made of 7 tons of heavy concrete having the weight density of 3.5 g/cc. There are eleven fast-neutron detectors. Each detector consists of a stilbene scintillator whose diameter/thickness is ϕ20 mm/10 mm and the photomultiplier tube with external gain stabilization power supply having the high gain stability over 10^6 cps range. The newly developed data acquisition system enables us to perform the online and offline neutron and gamma pulse shape analysis simultaneously even in the 10^6 cps region. The radial profile of the beam ion density can be obtained by the vertical neutron camera. The shot-integrated neutron emission amount is obtained by the neutron activation system consisting of two pneumatic capsule stations and two high-purity germanium semiconductor detectors [42]. By means of indium and silicon foils, the ratio of primary DD neutron emission yield and secondary DT neutron emission yield are obtained. The time resolved DT neutron emission rate is obtained by means of scintillating fiber detectors [43-47]. The scintillation fiber detectors consist of 10 cm long 1 mm ϕ BCF-10 fibers embedded into the Al substrate and the magnetic resistant photomultiplier tube. The triton burnup ratio evaluated by the scintillating-fiber detector absolutely calibrated by the neutron activation system is studied in order to understand the 1 MeV triton confinement as a demonstration of 3.5 MeV alpha particle confinement.

3. Global Beam Ion Confinement Study

Study of S_n on the deuterium NB heated deuterium plasma is performed in various magnetic configurations. Since, the LHD has high power and high energy N-NBs balanced injection into the plasma, the neutron emission caused by the so called beam-beam reaction could be relatively large fraction in S_n. Therefore, the beam-beam reaction fraction was evaluated [38]. The simulation result shows that the beam-beam component in both co- and counter-NBs injection case becomes 2.9 times higher than that in co-NB injection case. In these experiments, three negative-ion-based neutral beams (N-NBs) having the acceleration energy of up to 180 keV, and two positive-ion-based neutral beams (P-NBs) having the acceleration energy of up to 80 keV are injected with the power of 6 MW and 18 MW, respectively. Typical waveform of deuterium plasma discharge is shown in Fig. 2. The plasma was initiated by electron cyclotron heating (ECH) and three N-NBs from t of 3.3 s. The time-resolved analysis of S_n is performed using the TASK/FP code based on the Fokker Planck models [48, 49]. Note that the effective charge is assumed to be 1 and confinement time of the fast ions is assumed to be 0.4 s based on the NB blip experiment [50]. Here, the absolute value of S_n evaluated by TASK/FP code is normalized by S_n measured in the experiment. The time trend of S_n calculated by TASK/FP code agrees with the experiment. It is found that the beam-beam component fraction in S_n is approximately 20%. The beam-beam fraction in S_n is relatively high because in this experiment two N-NBs inject beams in co-direction, whereas the other NB injects beams in counter-direction. We surveyed S_n dependence on the line averaged electron density (n_{e_avg}) with n_{e_avg} changed from 1×10^{19} m^{-3} to 5×10^{19} m^{-3}. The maximum S_n in one shot as a function of n_{e_avg} in four different magnetic configurations are plotted in Fig. 3. The total neutron emission rate has a peak at n_{e_avg} of 2×10^{19} m^{-3} to 3×10^{19} m^{-3}, as predicted by Fokker-Planck models [18]. Here, the increase of S_n in the relatively low-density range is due to the improvement of the beam deposition, whereas the decrease of S_n in the relatively high-density

range is due to the decrease of the slowing down time induced by the lower electron temperature. The total neutron emission rate becomes lower with the outward shift of the magnetic axis position (R_{ax}) in the same density. The maximum value of S_n in the inward shifted configuration is approximately 3×10^{15} n/s, whereas in the outward shifted configuration S_n is approximately 3×10^{14} n/s. There is almost one order of difference. There are two possible reasons for this. One reason is due to the bulk plasma performance. In the LHD plasma, the plasma temperature tends to be higher in the inward shifted configuration compared with the outward shifted configuration with the same heating power and the plasma density. The higher-electron temperature provides the longer slowing time at the same plasma density. The other reason is due to the drift orbit of beam ions. In the inward shifted configuration, the guiding center orbit of helically trapped ions matched the flux surface. Therefore, confinement of helically trapped ions is predicted to be better in the inward shifted configuration compared with the outward shifted configuration. In addition, the deviation of the passing transit ion orbit from the flux surface becomes smaller in the inward shifted configuration compared with the outward shifted configuration. In order to understand the effect of the magnetic configuration and the plasma parameters on S_n, the calculation of beam-thermal neutron emission rate with considering the fast-ion-orbit effect in the short time period is performed using FIT3D-DD code [51]. Here, the orbit following time is set to be 0.1 ms and the effective ion charge is set to be 1. The maximum S_n by calculation at R_{ax} of 3.55 m is 6.4×10^{15} n/s, which is almost two times higher than the experimental value. The calculated S_n by FIT3D-DD shows that the S_n has a peak at n_{e_avg} of 2×10^{19} to 3×10^{19} m^{-3} as obtained in the experiment. Although the absolute value of S_n is almost two times higher in the FIT3D-DD code, the trend of S_n on n_{e_avg} agrees with that obtained in the experiments. One of the possible reasons of discrepancy in absolute value of S_n is effective charge of the plasma. In this calculation, the effective charge was

assumed to be one. By including larger and realistic effective charge, the difference between experiment and FIT3D-DD result becomes less.

The fusion gain, which is the ratio of the fusion output divided by the total injection power is surveyed with the deuterium N-NB heated deuterium plasmas. In these discharges, no ECH and no P-NBs are injected into the plasma. The fusion gain of a deuterium plasma is defined as Q_{DD}= (S_n×7.25 MeV)/($P_{N\text{-}NB\_dep}$) in these discharges, where $P_{N\text{-}NB\_dep}$ represents the deposition power of N-NBs. The dependence of Q_{DD} on the deposition power is surveyed in the normal B_t (2.75 T) and half B_t (1.375 T) cases in R_{ax} of 3.60 m. The higher Q_{DD} is obtained in the normal B_t case compared with the half B_t case, as expected (Fig. 4(a)). The fusion gain increases as $P_{N\text{-}NB\_dep}$ until 3 MW, and then the fusion gain becomes relatively flat in both cases. Q_{DD} reaches 4×10^{-4} in $P_{N\text{-}NB\_dep}$ of 3.5 MW. The equivalent fusion gain in DT plasma Q_{DT} is evaluated using the FBURN code which is based on the classical beam ion confinement assumption [52]. In the case of deuterium beam injection to triton plasma, Q_{DT}/Q_{DD} is 249, whereas Q_{DT}/Q_{DD} is 164 in the case of triton beam injection to deuterium plasma. Note that the reason for higher Q_{DT}/Q_{DD} in deuterium beam injection to triton plasma compared with triton beam injection to deuterium plasma is higher relative velocity in the case of deuterium beam injection. It is worth noting that the value of Q_{DT}/Q_{DD} is almost the same as Q_{DT}/Q_{DD} obtained in TFTR [53]. The maximum equivalent Q_{DT} in the first campaign of the LHD deuterium experiment is 0.11 which is almost the same value obtained in large tokamaks with approximately 5 MW NB injections [53-55]. The dependence of Q_{DD} on the plasma parameters is surveyed. It is found that that the Q_{DD} linearly increases with $T_{e0}^{1.5}$ (Fig. 4(b)). In the NB-heated LHD plasmas, neutrons are mainly created by a beam-plasma reaction. Therefore, the fusion gain can be approximately expressed as $Q_{DD} \sim S_n/P_{NB} \sim n_i \times P_{NB} \times \tau_s/P_{NB} \sim n_i \times T_e^{1.5}/n_e \sim T_e^{1.5}$. Figure 4 (b) insists that neutrons are mainly created by a beam-thermal reactions, as expected.

We performed NB blip experiments with P-NB injection having the acceleration voltage of 55 kV into the ECH plasma in order to study the beam ion confinement. In this experiment, n_{e_avg} is approximately 1.5×10^{19} m^{-3} and the central electron temperature is 3 keV. The injection power of ECH and NB are 0.8 MW and 7 MW, respectively. The total neutron emission rate increases rapidly with P-NB injection, and then decays due to the switch off of P-NB. The decay of S_n is due to the slowing down and transport/loss of beam ions. The time evolution of S_n measured in experiment shows that the decay time of S_n is 215 ms. Time evolution of S_n obtained with the experiment is compared with the numerical simulation using the five-dimensional drift kinetic equation solver based on the Boozer coordinates, the Global NEoclassical Transport (GNET) code [56], and the FBURN code with no radial diffusion using the experimental data (Fig. 5). Here, S_n calculated by FBURN is normalized at when P-NB turned off. Note that in GNET code, transport of beam ions due to the collision and orbit effect is included, whereas in the FBURN code, beam ions are slowdown without moving from the deposited position. The rise time of S_n calculated by the FBURN code is almost the same as that of the GNET code. On the other hand, the decay time of S_n calculated by the FBURN code is longer than that calculated by GNET code. The decay time of S_n calculated by the FBURN code is 250 ms, whereas the decay time of S_n calculated by the GNET code is 216 ms. The decay time becomes shorter in the GNET result compared with the FBURN result because of the diffusion of the beam ions. It is found that not only the decay time of S_n, but also the absolute value of S_n matched with that obtained in the experiments. Therefore, the confinement of beam ions created by NB blip in the low-beta MHD quiescent plasma can be described with the neoclassical models.

4. Study of Beam Ion Profile

The neutron emission profile measurement in N-NB heated deuterium plasma using the vertical neutron camera is performed in three different magnetic axis configurations. In this experiment, an N-NB (NB#3) is injected into the ECH plasma (Fig.6 (a)). The injection power of ECH and the deposition power of N-NB are up to 3 MW and up to 1 MW, respectively. The central electron temperature and n_{e_avg} are up to 7 keV and 1.2×10^{19} m^{-3}, respectively. The neutron counts of the vertical neutron camera increase due to the increase of the deposition power of the N-NB. Here, the error of neutron counts is due to the statistical error in the counts. The neutron counts in the central chord shows relatively high counting rate compared with the neutron counts in the edge channel. The neutron emission profile becomes stable after t of 3.7 s. We plotted the line-integrated neutron emission profile at t of 3.7 s to 4.3 s in R_{ax} of 3.60 m, 3.75 m, and 3.90 m, respectively. The line-integrated neutron emission profile shown in Fig. 6 (b) indicates that the neutron counts increase as the inward shift of R_{ax}. This tendency is consistent with the dependence of S_n on R_{ax} shown in Fig. 3. The peak position of the neutron counts changed according to R_{ax}. The line-integrated neutron profile is predicted by the MORH code which is based on the Monte Carlo guiding center orbit following models [57] using the equilibrium reconstructed by the HINT code [58]. In this calculation the birth profile of beam ions is calculated by HFREYA code which is a part of the FIT3D code [51]. The effective charge is assumed to be 1. We follow the orbit until beam ions thermalize. The temperature and density profile is given according to the measurement by Thomson scattering diagnostics [59]. The beam-thermal neutron emission is calculated based on Mikkelsen's formula [60] using the fusion cross section in Ref. 61. Here, the neutron emission due to the beam-beam components is not included because the fraction of beam-beam components on S_n is negligibly small due to the low relative velocity between beam ions injected into the same direction. Two dimensional neutron emissivity profile together with the plasma shape in the vertical elongated

cross section where the vertical neutron camera installed is shown in Fig. 6 (c). The maximum neutron emissivity in the plasma core is slightly less than 2×10^{14} $s^{-1}m^{-3}$. Note that S_n calculated by MORH is consistent with the S_n calculated by the FIT3D-DD code. The peak position of the neutron emissivity appears slightly outward compared with R_{ax} position. The shift of the neutron emissivity outward is due to the outward shift of the orbit from the flux surface for co-passing transit beam ions. The line-integrated neutron profiles predicted by MORH code are shown in Fig. 6 (d). The peak value of neutron counts is almost two times higher than that of the experiments. The peak position of the neutron counts changed according to R_{ax}. The position is comparable to the peak position obtained in experiments. Note that in the calculation the line-integrated neutron emission profile is narrower compared with experiments. The one possibility of a narrower profile is due to the effective charge. The larger effective charge might enhance the pitch angle scattering which causes the profile breadth.

5. Confinement of MeV Ion

The confinement of MeV ion is one of the key topics especially in the stellarators and the helical devices. The triton burnup study is performed for the first time in stellarator and helical devices. The triton burnup ratio is defined as S_{n_DT}/S_{n_DD}, where S_{n_DT} and S_{n_DD} represent total DT neutron emission rate and total DD neutron emission rate, respectively. To measure the secondary DT neutron emission caused by bulk deuterium and 1 MeV triton born by DD reaction, we developed a scintillating-fiber detectors [43]. The initial results showed that the diffusion of 1 MeV triton is around 0.2 m^2/s, which is same order as that in the large tokamaks 55]. The triton burnup experiments are performed in R_{ax} from 3.55 m to 3.90 m by the scintillating fiber detector calibrated by the neutron activation system. The typical waveform of the triton burnup experiment is shown in Fig. 7 (a). The plasma is heated by the electron

cyclotron heating and N-NB injections having the acceleration energy of up to 180 keV. The line averaged density rises to 2×10^{19} m^{-3}, then becomes flat from t=4.0 s, and then begins decreasing from t=5.3 s. The total neutron emission rate sharply increases due to the N-NB injections from t=3.3 s, and then starts decreasing from t=5.3 s. There are two decay component in S_n from t=5.3 s. The relatively fast decay component mainly corresponds to the slowing down and the diffusion of the beam ions, whereas the relatively slow component corresponds to the slowing down and the diffusion of the tritons. Note that the time trace of S_n measured by the neutron flux monitor matches the S_{n_DT} measured by the scintillating fiber detector. The triton burnup ratio as a function of R_{ax} obtained in experiments shown in Fig. 7 (b) indicates that the triton burnup ratio substantially increases with the inward shift of R_{ax}. Here, the different triton burnup ratio obtained in each R_{ax} condition is due to the different density and temperature. The maximum triton burnup ratio achieved in the first deuterium campaign in the LHD is 0.45%, which is a similar value to that obtained in middle-sized tokamaks whose minor radius is comparable to the LHD, such as TFTR and KSTAR [62, 63]. The triton burnup ratio is evaluated using the GNET code in R_{ax} of 3.5 m, 3.6 m, and 3.75 m (Fig. 7 (c)). The calculation result shows that the triton burnup ratio increases with the inward shift of R_{ax}, as obtained in experiments. However, the absolute value of the triton burnup ration is lower than the value obtained in experiments. The difference of the evaluated triton burn up ratio by the GENT from the experiment result comes from the finite Larmor radius and re-entering effects because the guiding center orbit of triton is followed in the Boozer coordinates in GNET code.

6. Summary

The research on the energetic particle confinement has progressed by means of comprehensive neutron diagnostics installed for the deuterium operation of the LHD plasma. The total neutron

emission rate dependence on electron density shows that S_n has a peak around n_{e_avg} of 2×10^{19}-3×10^{19} m^{-3} as predicted by the Fokker-Planck code and the FIT3D-DD code. TASK/FP shows that the ratio of total beam-beam neutron on S_n in the three N-NBs heated plasma is approximately 20%. The fusion gain of the N-NB heated deuterium plasma is evaluated to be 4.0×10^{-4}, which is comparable with the value obtained in the large tokamak with similar heating power. The equivalent Q_{DT} of 0.11 is calculated by FBURN code using the experimental data. The NB blip experiments are performed in electron cyclotron heated plasma with P-NB injection. Not only the decay time of S_n but also the absolute value of S_n matched with the GNET code. The result indicates that transport of beam ion injected by short pulse NB in magnetohydrodynamic quiescent low-beta plasmas can be described with the neoclassical model. Neutron emission profile from stellarators and helical devices is obtained for the first time. The line-integrated neutron emission profile shows that the peak of the profile shifted outward, as expected by MORH code. The triton burnup experiment is performed in various magnetic field configurations. This is the first triton burnup experiment in stellarators and helical devices. It is found that the triton burnup ratio increases considerably with the inward shift of the magnetic axis in both experiment and numerical simulation.

Acknowledgements

This research was supported by NIFS Collaboration Research programs (KOAH033), and by the LHD project budget (ULHH003, ULHH034, ULHH802, and ULGG801).

References

[1] Fasoli A. et al 2007 Nuclear Fusion **47** S264.

[2] Heidbrink W. W. and Sadlers G. 1994 J. Nuclear Fusion **34** 535.

[3] Morisaki T. et al "Overview of the First Deuterium Experiment in LHD", IAEA Fusion Energy Conference, Gandhinagar, India, 2018.

[4] Dinklage A. et al 2018 Nature Physics **14** 855.

[5] Osakabe M. et al 2010 Fusion Science and Technology **58** 131.

[6] Toi K. et al 2010 Fusion Science and Technology **58** 186.

[7] Toi K. et al 2011 Plasma Physics and Controlled Fusion **53** 024008.

[8] Isobe M. et al 2010 Fusion Science and Technology **58** 426**.**

[9] Ogawa K. et al 2008 Plasma and Fusion Research **3** S1082.

[10] Ogawa K. et al 2009 Journal of Plasma and Fusion Research SERIES **8** 655.

[11] Osakabe M. et al 2006 Nuclear Fusion **46** S911.

[12] Ogawa K. et al 2010 Nuclear Fusion **50** 084005.

[13] Isobe M. et al 2010 Contributions to Plasma Physics **50** 540.

[14] Ogawa K. et al 2012 Plasma Science and Technology **14** 269.

[15] Ogawa K. et al 2012 Nuclear Fusion **52** 094013.

[16] Ogawa K. et al 2014 Plasma Physics and Controlled Fusion **56** 094005.

[17] Iiyoshi A. et al 1990 Fusion Technology **17** 169.

[18] Osakabe M. et al 2017 Fusion Science and Technology **72** 199.

[19] Homma M. et al 2015 Plasma and Fusion Research **10** 3403050.

[20] Seki R. et al 2018 "*Evaluation of Neutron emission rate with FIT3D-DD code in large helical device*", The 27th International Toki Conference on Plasma and Fusion Research & the 13th Asia Pacific Plasma Theory Conference (2018) **P1-19** and to be submitted Plasma and Fusion Research.

[21] Isobe M. et al 2014 Review of Scientific Instruments **85** 11E114.

[22] Nakano Y. et al 2014 Review of Scientific Instruments **85** 11E116.

[23] Nakano Y. et al 2014 Plasma and Fusion Research **9** 3405141.

[24] Nishitani T. et al 2017 Fusion Engineering and Design **123** 1020.

[25] Ogawa K. et al 2014 Review of Scientific Instruments **85** 11E110.

[26] Uchida Y. et al 2014 Review of Scientific Instruments **85** 11E118.

[27] Uchida Y. et al 2017 Review of Scientific Instruments **88** 083504.

[28] Ogawa K. et al 2018 Review of Scientific Instruments **89** 095010.

[29] Isobe M. et al 2013 Plasma and Fusion Research **8** 240268.

[30] Tomita H. et al 2013 Plasma and Fusion Research **8** 2406095.

[31] Nakayama Y. 2015 Physics Procedia **80** 81.

[32] Izumi Y. et al 2016 Review of Scientific Instruments **87** 11E728.

[33] Yamamoto Y. et al 2014 Progress in Nuclear Science and Technology **4** 679.

[34] Tomita H. et al 2014 Review of Scientific Instruments **85** 11E120.

[35] Takada E. et al 2016 Plasma and Fusion Research **11** 2405020.

[36] Takada E. et al submitted to Review of Scientific Instruments.

[37] Amitani T. et al 2018 "*Development of Fast-Neutron Detector with Scintillating Optical Fiber for Triton Burnup Experiment in Deuterium Plasmas*", The 27th International Toki Conference on Plasma and Fusion Research & the 13th Asia Pacific Plasma Theory Conference (2018) **P2-13**.

[38] Homma M. et al 2016 Plasma and Fusion Research **11** 2403109.

[39] Isobe M. et al 2018 Nuclear Fusion **58** 082025.

[40] Isobe M. et al 2018 IEEE Transactions on Plasma Science **46** 2050.

[41] Nishitani T. et al 2018 Fusion Engineering and Design **136 Part A** 210.

[42] Pu N. et al 2017 Review of Scientific Instruments **88** 113302.

[43] Ogawa K. et al 2018 Nuclear Fusion **58** 034002.

[44] Wurden G. A. et al 1995 Review of Scientific Instruments **66** 901.

[45] Nishitani T. et al 1996 Plasma Physics and Controlled Fusion **38** 355.

[46] Pu N. et al 2018 Review of Scientific Instruments **89** 1111105.

[47] Pu N. et al 2018 Plasma and Fusion Research **13** 3402121.

[48] Nuga H. and Fukuyama A. 2011 Progress in Nuclear Science and Technology **2** 78

[49] Nuga H. et al 2019 Nuclear Fusion **59** 016007.

[50] Nuga H. et al "Analysis of energetic particle confinement in LHD using neutron diagnostics and Fokker-Planck codes", The 27th International Toki Conference on Plasma and Fusion Research & the 13th Asia Pacific Plasma Theory Conference (2018) **P2-14** and to be submitted Plasma and Fusion Research.

[51] Murakami S. et al 1995 Transactions of Fusion Technology **27** 256.

[52] Ogawa K. et al 2018 Plasma Physics and Controlled Fusion **60** 9.

[53] Jassby D. L. et al 1991 Physics of Fluids B: Plasma Physics **3** 2308.

[54] Keilhacker M. and the JET Team 1990 Physics of Fluids B: Plasma Physics **2** 1291.

[55] Nishitani T. et al 1994 Nuclear Fusion **34** 1069.

[56] Murakami S. et al 2002 Nuclear Fusion **42** L19.

[57] Seki R. et al 2015 Plasma and Fusion Research **10** 1402077.

[58] Suzuki Y. et al 2003 Plasma Physics and Controlled Fusion **45** 971.

[59] Yamada I. et al 2010 Fusion Science and Technology **58** 345.

[60] Mikkelsen D. et al 1989 Nuclear Fusion **29** 1113.

[61] Bosch H. S. and Hale G. 1992 Nuclear Fusion **32** 611.

[62] Hoek M., Bosch H. S. and Ullrich W. 1999 "Triton burnup measurement at ASDEX Upgrade by neutron foil activation", IPP-Report IPP-1/320.

[63] Jo J. et al 2016 Review of Scientific Instruments **87** 11D828.

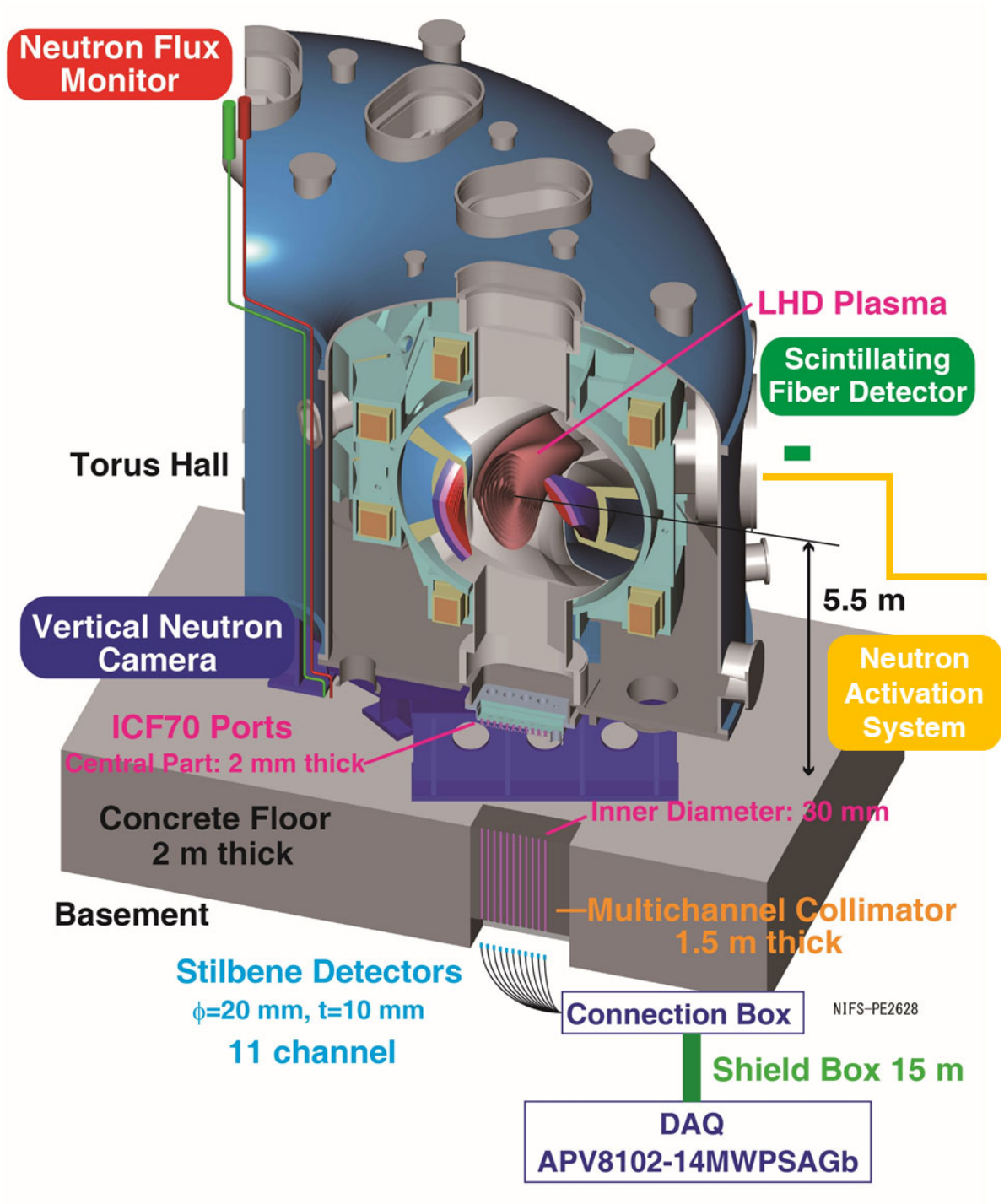

Fig. 1 The schematic drawing of the Large Helical Device. The neutron flux monitor, the neutron activation system, the vertical neutron camera, and the scintillating-fiber detector are installed.

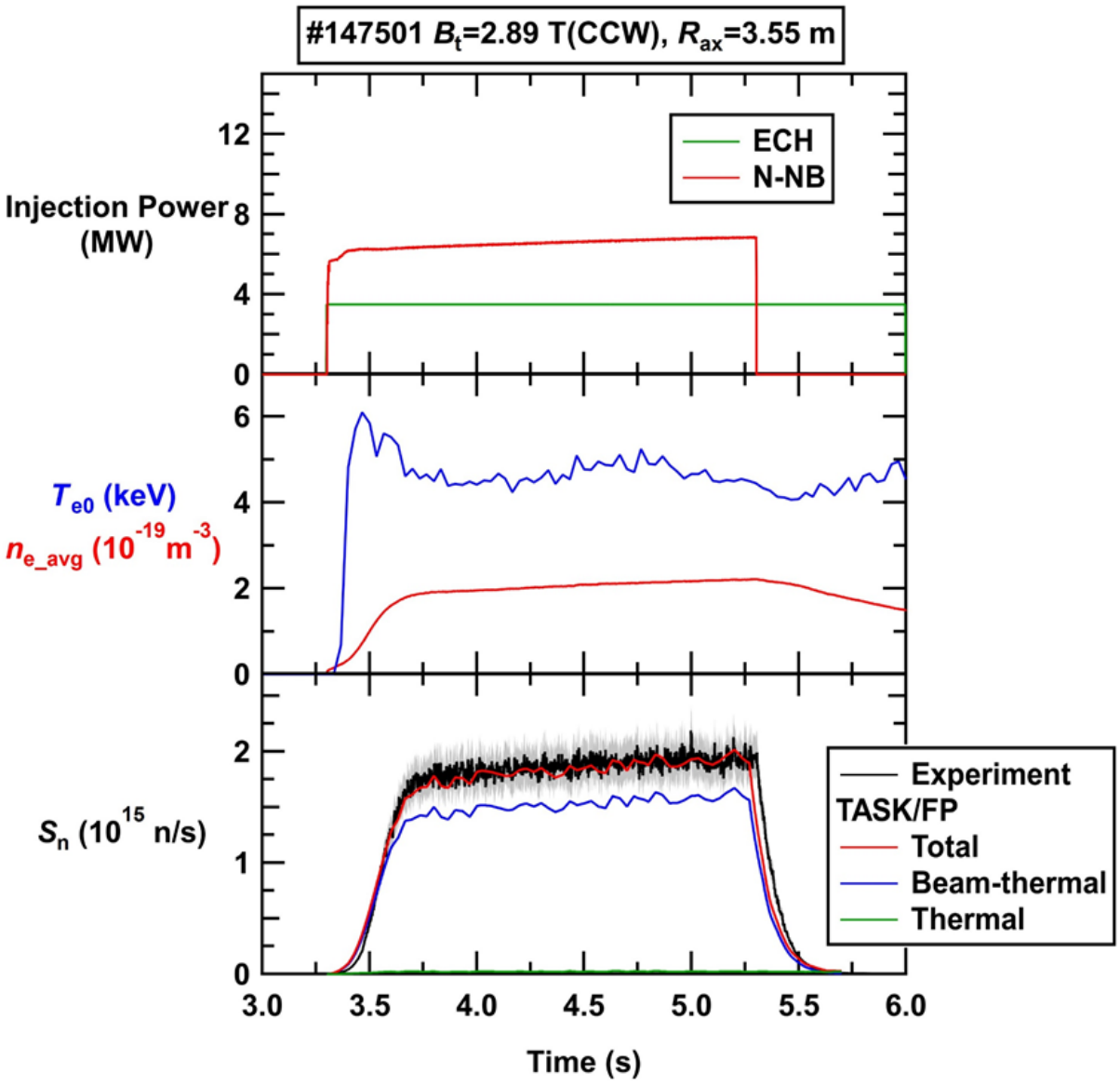

Fig. 2 Typical time evolution of a deuterium plasma discharge performed in LHD. Here, a plasma is heated by ECH and three N-NB. The time trend of S_n is predicted by TASK/FP code based on the plasma parameter obtained in the experiment. Here, absolute value of S_n in TASK/FP is normalized to the experimental value. From TASK/FP code analysis, neutron emission from beam-plasma reaction is dominant in S_n. The beam-beam fraction in S_n is around 20%.

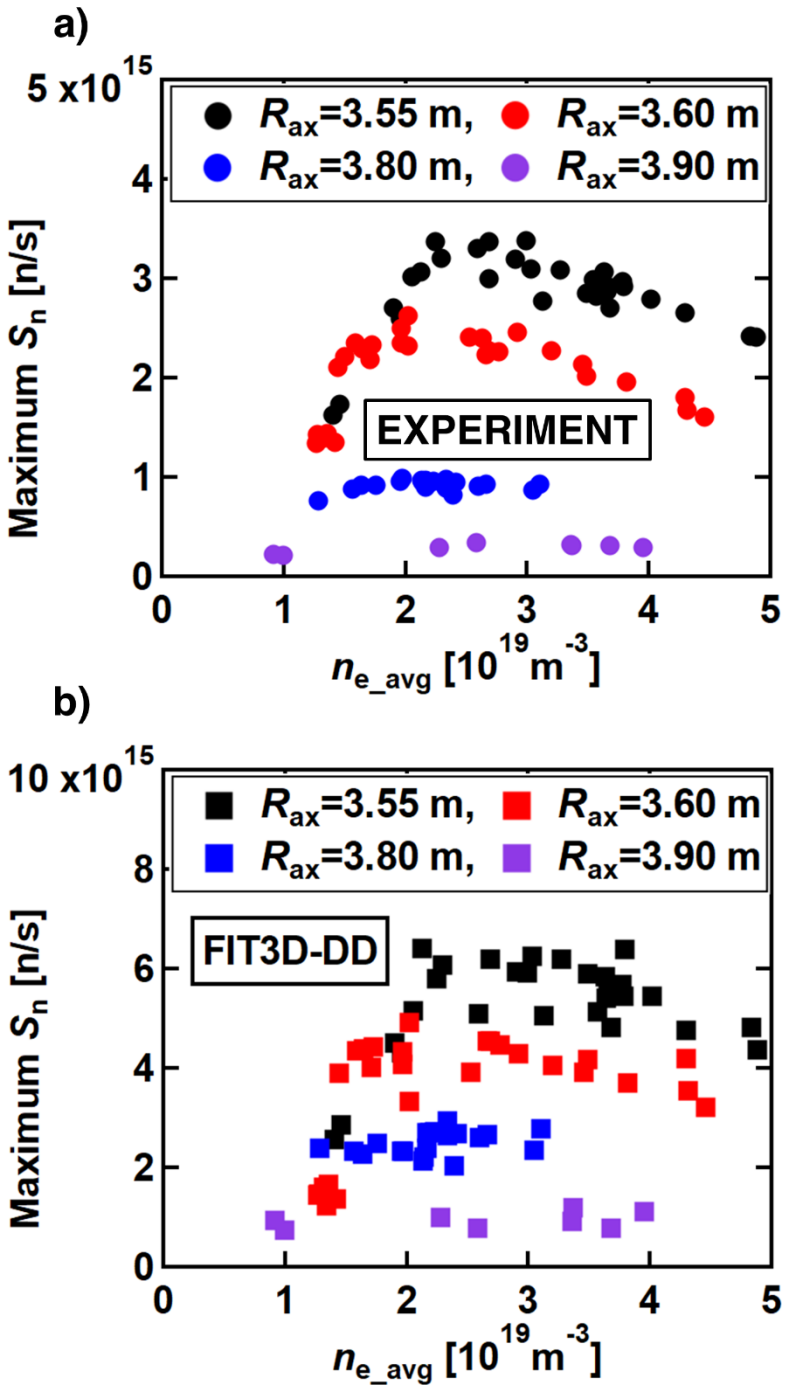

Fig. 3 The dependence of the maximum total neutron emission rate in one shot on the line averaged density. The total neutron has the peak at around the density of 2×10^{19} m^{-3} to 3×10^{19} m^{-3}. Although the absolute value of S_n evaluated by the FIT3D-DD code is two times higher than an experiment, the dependence of S_n in n_{e_avg} is successfully reproduced.

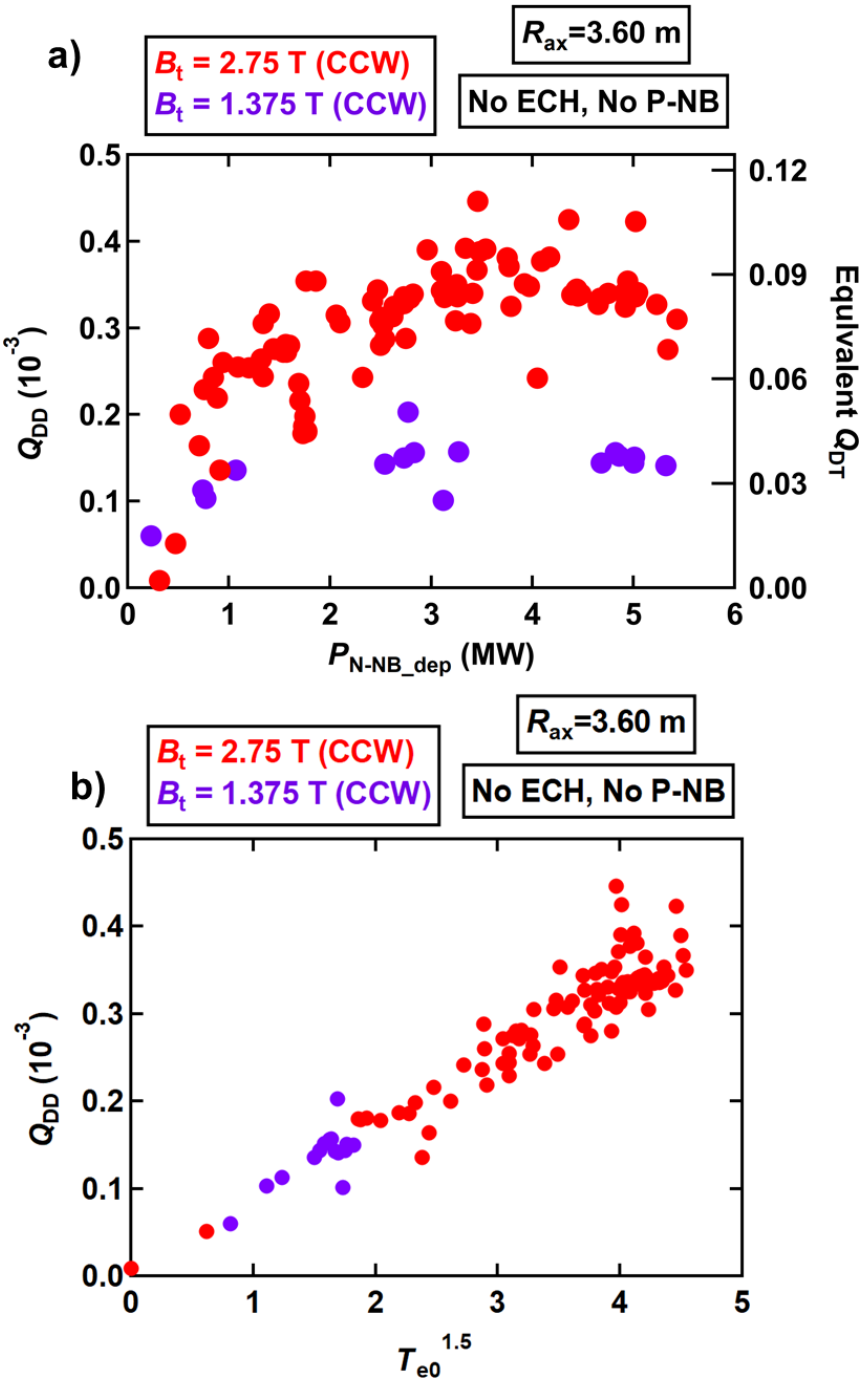

Fig. 4 (a) Q_{DD} as a function of absorbed power of N-NB injection measured in the experiment. Higher Q_{DD} can be obtained in higher magnetic field strength configuration, as expected. The equivalent Q_{DT} of 0.11 is achieved. Here, the ratio of Q_{DD} and equivalent Q_{DT} is evaluated by FBURN code. (b) Q_{DD} as a function of $T_{e0}^{1.5}$. Q_{DD} proportionate to $T_{e0}^{1.5}$ showing that neutrons are mainly created by beam-thermal reactions.

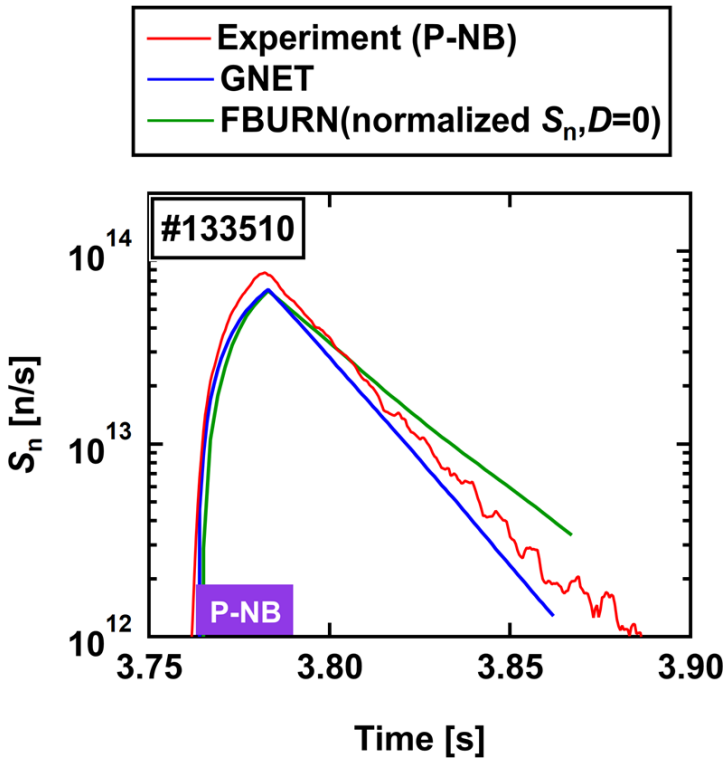

Fig. 5 Time evolution of S_n in P-NB blip in experiment, calculated by the one-dimensional simulation based on classical confinement without radial diffusion (FBURN), and the five-dimensional neoclassical transport code (GNET). The decay time of S_n becomes shorter due to the diffusion of beams. The time trace of total neutron emission rate successfully reproduced by GNET calculation.

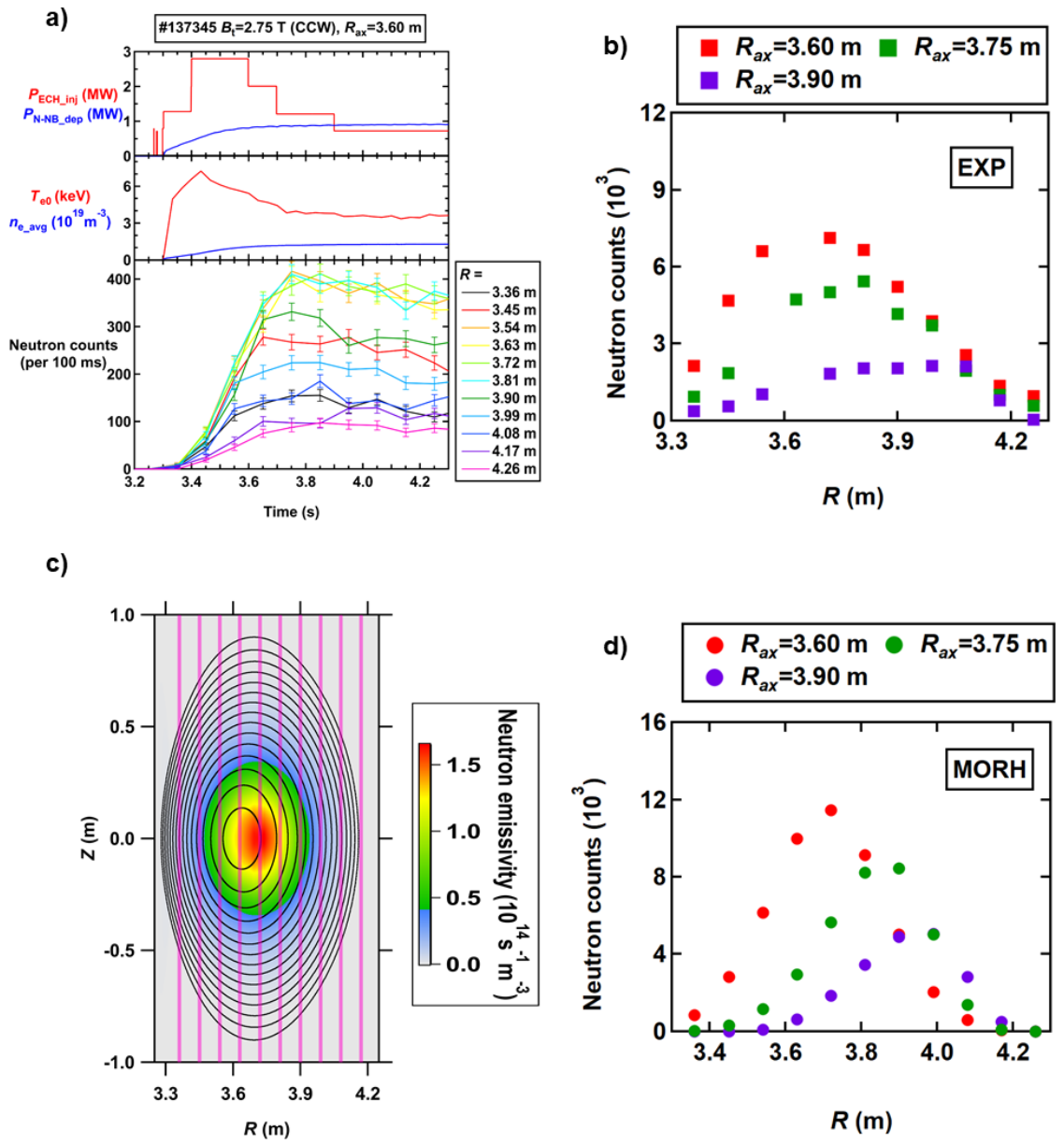

Fig. 6 (a) Time evolution of the injection power of electron cyclotron heating, deposition power of neutral beam injection, the central electron temperature measured by Thomson scattering diagnostics, the line averaged electron density measured with the interferometer, and the line-integrated neutron emission profile measured by the vertical neutron camera. (b) Line-integrated neutron emission profile measured by the vertical neutron camera. The neutron count increases with the inward shift of the magnetic axis. The peak of neutron counts changes according to the magnetic axis, as expected. (c) Two-dimensional neutron emissivity obtained from MORH code in the vertically elongated poloidal cross section where the vertical neutron camera is installed. (d) Line-integrated neutron emission profile calculated by the MORH code. The absolute neutron count is the same order as the count in the experiment. The shift of the neutron counts peak according to the magnetic axis is reproduced.

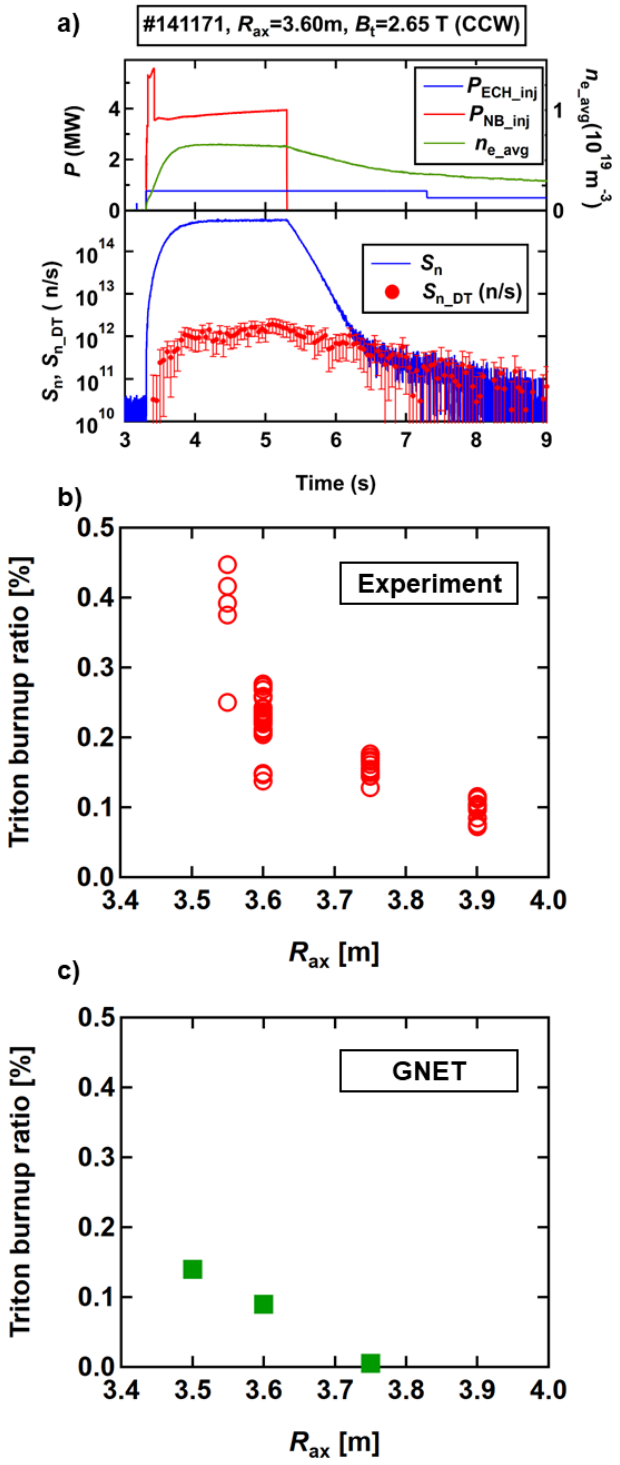

FIG. 7. (a) Typical time trace of triton burnup discharge. The evolution of injection power of electron cyclotron heating, injection power of neutral beam injections, the line averaged electron density measured with interferometer, the total neutron emission rate measured with the neutron flux monitor, and total DT neutron emission rage measured with the scintillating fiber detectors are shown. (b) Triton burnup ratio as a function of the magnetic axis position obtained in experiments. Triton burnup ratio dramatically increased with the inward shift of magnetic axis. (c) Triton burnup ratio evaluated by GNET code. An increase of the triton burnup ratio with the inward shift of magnetic axis is reproduced by the GNET calculation.

Appendix The list of codes to evaluate neutron emission rate

Code	Input	Model	Orbit effect	Dimension	Collision model
FBURN	T_e profile, n_e profile, Equilibrium, and beam deposition	Classical EP confinement	No	1 (velocity) + 1 (space)	Slowing down
FIT3D-DD		Steady state solution of Fokker-Planck	Guiding center within 0.1 ms	2 (velocity) + 1 (space)	Slowing down
TASK/FP		Fokker-Planck	Guiding center within 0.1 ms	2 (velocity) + 1 (space)	Nonlinear Coulomb collision
MORH		Drift kinetic	Guiding center	2 (velocity) + 3 (space)	Liner Coulomb collision
GNET		Drift kinetic	Guiding center	2 (velocity) + 3 (space)	Nonlinear Coulomb collision